Results of Preliminary Clinical Trials of the Positron Emission Mammography System PEM-I: A Dedicated Breast Imaging System Producing Glucose Metabolic Images Using FDG

Kavita Murthy, Marianne Aznar, Christopher J. Thompson, Antoine Loutfi, Robert Lisbona, and Jean H. Gagnon

Montreal Neurological Institute, Medical Physics Unit, and Royal Victoria Hospital, McGill University, Montreal, Quebec, Canada

Early detection of breast cancer is crucial for efficient and effective treatment. We have developed an instrument for positron emission mammography (PEM) called PEM-I that performs high-resolution metabolic imaging of breast cancer. Images of glucose metabolism are obtained after injection of 75 MBq FDG. The PEM detectors are integrated into a conventional mammography system, allowing acquisition of the emission images immediately after the mammogram, without subject repositioning, and accurate coregistration of images from the 2 modalities. In this article, we present the results of the first clinical pilot study with the instrument. **Methods:** Sixteen subjects (age range, 34–76 y) were studied. All subjects were nondiabetic, nonpregnant, and without a history of cancer. They had recently been found to have suggestive mammography findings or a palpable breast mass and underwent lumpectomy or mastectomy within 2 wk of the study. Results from the PEM study were compared with those from mammography and pathology. A PEM test was classified positive (indicating the presence of cancer) if significant focal uptake was seen in the image or if the counting rate in the breast with suggestive findings was significantly higher than in the contralateral breast. **Results:** Of the 16 subjects studied, 14 were evaluable. Ten cancerous tumors and 4 benign tumors were confirmed by pathologic examination after complete removal of the tumor. PEM correctly detected the presence of disease in 8 of 10 subjects. Findings were false-negative in 2 instances and false-positive in none, giving the instrument 80% sensitivity, 100% specificity, and 86% accuracy. **Conclusion:** Our preliminary results suggest that PEM can offer a noninvasive method for the diagnosis of breast cancer. Metabolic images from PEM contain unique information not available from conventional morphologic imaging techniques and aid in expeditiously establishing the diagnosis of cancer. In all subjects, the PEM images were of diagnostic quality, with an imaging time of 2–5 min.

Key Words: PET; FDG; breast cancer; metabolic imaging

J Nucl Med 2000; 41:1851–1858

Received Jun. 16, 1999; revision accepted Nov. 1, 1999.

For correspondence or reprints contact: Christopher J. Thompson, DSc, Montreal Neurological Institute No. 798, 3801 University St., Montreal, Quebec H3A 2B4 Canada.

Breast cancer is the second most common cause of cancer mortality among women in industrialized countries (*1*). Early diagnosis is widely acknowledged as being crucial in the successful treatment of the disease (*2*). Clinical trials have shown a significant increase in the 5-y survival rate if the cancer is detected in its early stage (stage I) (*3*). Mammographic sensitivity in premenopausal women, who typically have dense breasts, is less than in older women, whose breasts are relatively more radiolucent. As reported by Kerlikowske et al. (*4*), mammographic sensitivity is 93.2% for postmenopausal women and 83.6% for premenopausal women. One of the contributing factors for this lowered sensitivity is the relatively higher numbers of false-negative mammography findings for women in the 40- to 49-y age group (*5*).

Metabolic imaging techniques detect physiologic rather than structural changes associated with malignant tumors. In recent years, metabolic imaging techniques such as PET and SPECT have found widespread oncologic use because of their high sensitivity and specificity (*6–10*). Enhanced glucose metabolism of untreated malignant tumors was first reported by Warburg et al. in 1930 (*11*). Whole-body PET with radiolabeled FDG, in particular, has been used to successfully detect a wide variety of cancer, including breast cancer (*12–15*).

FDG is a positron-emitting glucose analog and, like glucose, is cell membrane permeable. The process of glycolysis phosphorylates the FDG to FDG-6-phosphate, most of which remains trapped in the cell without undergoing further metabolism. Cells with increased glucose metabolism have greater FDG accumulation and therefore send out stronger signals than do their normal counterparts. Wahl et al. (*15*) have reported a median tumor-to-background ratio of 8:1 in the breast in whole-body FDG PET studies.

Several groups have successfully used whole-body PET technology with FDG as the radiotracer for the detection of breast cancer. Wahl et al. (*15*), in 1991, reported 100% sensitivity for attenuation-corrected whole-body PET using 370 MBq FDG. Crowe et al. (*16*), in 1994, reported 96%

sensitivity and 100% specificity with the same dose of FDG. Recently, Avril et al. (*17*,*18*) reported a sensitivity in the range of 68%–94% and a specificity of 84%–97% with a similar dose of FDG. Current state-of-the-art whole-body PET instruments have an in-plane spatial resolution of 5 mm full width at half maximum at best. Early-stage breast cancers are less than 2 cm in diameter and so may not be visible on a whole-body PET scan. Various designs have been proposed for high-resolution dedicated breast imaging systems that use PET or SPECT technology (*19*–*23*). Our positron emission mammography (PEM) instrument is based on the prototype design first proposed by Thompson et al. (*24*) in 1994. The first clinical PEM case study was reported by Weinberg et al. (*23*) in 1996.

MATERIALS AND METHODS

System Description

The PEM system at our laboratory consists of 2 planar detectors that are positioned 1 above and 1 below the breast (*25*). Each detector consists of 4 pixilated bismuth germanate blocks optically coupled to position-sensitive photomultiplier tubes (R3941–05 PS-PMT; Hamamatsu, Bridgewater, NJ) with a 72 × 72 mm entrance window and a useful field of view (FOV) of 65 × 55 mm. (The FOV is greater in 1 direction because the crossed-wire anode design of the PS-PMT has an 18 × 16 wire grid for position discrimination (*26*).) The completed system has a spatial resolution of 2.8 mm full width at half maximum. A tumor uptake ratio of 6:1 (tumor-to-background ratio) is required to produce images with visually identifiable uptake (image contrast of 1.86:1 [tumor-to-background ratio]). Tumors with smaller uptake ratios cannot be visually distinguished from the background (*27*). Robar et al (*28*) have described the detectors in detail.

Figure 1 is a photograph of the PEM-I system detectors installed on a standard conventional mammography system set up for a craniocaudal view. The detector assembly is mounted on a standard mammographic magnification table that attaches to the gantry of a Mammo Diagnost-UC system (Philips, Danbury, CT). The 2 detectors are attached to a support pole and can move in tandem in the horizontal direction. The upper detector can slide on the support pole so that the detector separation can be adjusted to match the thickness of the compressed breast. The entire detector assembly can be rotated with the gantry of the mammography unit to acquire PEM images in the mediolateral oblique position if required.

Figures 2A and B illustrate detector positioning for the acquisition of the mammogram and emission image, respectively. During the acquisition of the mammogram, the PEM detectors remain outside the FOV of the x-rays (Fig. 2A). During acquisition of the emission image, the PEM detectors are positioned over the compressed breast (Fig. 2B). This arrangement allows acquisition of mammograms and emission FDG PEM images without subject repositioning and facilitates accurate coregistration of images from the 2 modalities (*29*). A coregistration tool in the form of a steel wire frame (visible on the mammogram) is attached to the upper detector to allow precise positioning of the PEM detectors over the breast. The area enclosed by the wire frame is nominally equal to the useful FOV of the PEM system. The sides of the rectangular frame have regularly spaced markers that are used for scaling emission images to match the size of the mammograms.

Data Acquisition and Image Formation

The 2 detectors operate in coincidence, and data are collected in list mode. Figure 3 illustrates the sequence of events leading to the formation of images. On the detection of a coincidence event, the PEM electronics decode the raw x and y coordinates of the coincidence on opposing PS-PMT faces. These values are corrected for the spatial distortion and efficiency to obtain the correct x and y coordinates. A line of response (LOR) is drawn joining the points of interaction. The breast volume between the detectors is divided by 7 equidistant planes. The point of interaction of the LOR with each of the 7 planes is determined (*30*). A number (whose value is inversely proportional to the product of the probability of detection of an annihilation in that plane, the crystals' efficiencies, and the γ-ray attenuation along the path to the crystal) corresponding to the crystal element identified is added to the image matrix. Seven image frames corresponding to the 7 slices are displayed across the screen, with the leftmost frame corresponding to the

FIGURE 1. Photograph of PEM-1 system installed in mammography unit at Cedars' Breast Clinic. Lower detector is housed in standard mammographic magnification table and positioned below breast. Upper detector is positioned above compression paddle.

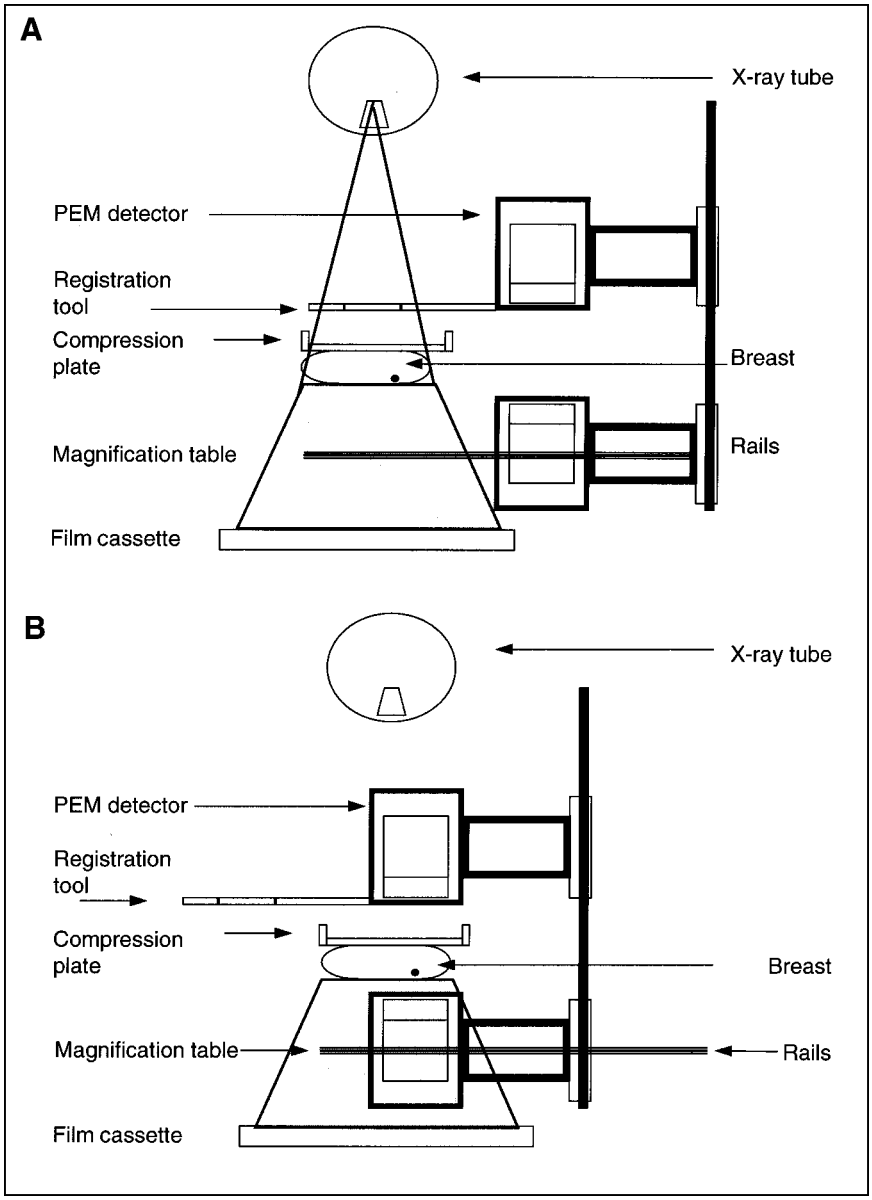

FIGURE 2. Schematics showing position of PEM detectors during acquisition of mammogram (A) of breast and emission scan (B) of breast. During mammogram, coregistration tool occupies position of PEM detectors. During emission scan, detectors replace coregistration tool.

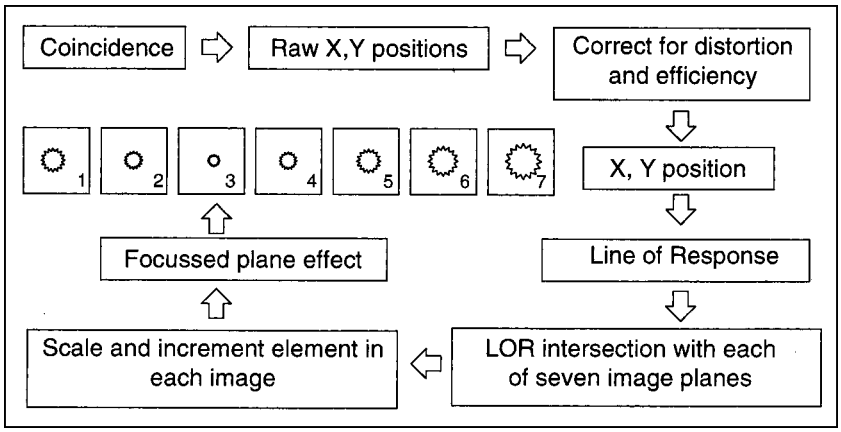

FIGURE 3. Basic principles of data acquisition and limited-angle backprojection used in formation of PEM images. Planar PEM images are displayed in sets of 7 frames, with leftmost frame corresponding to slice closest to upper detector.

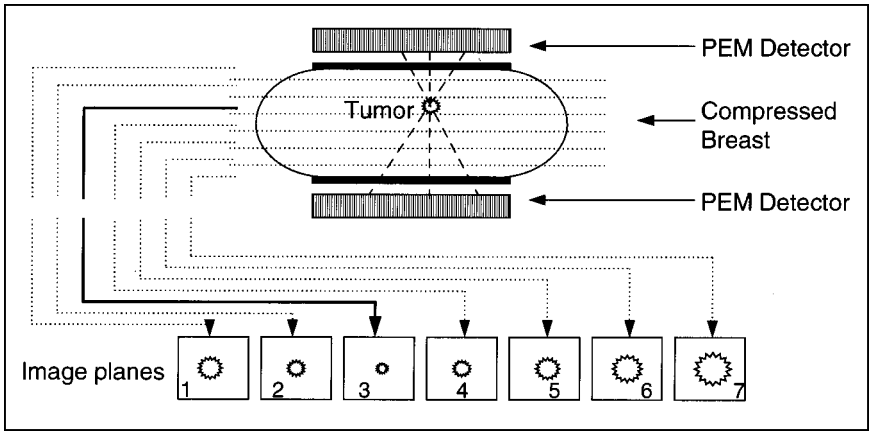

FIGURE 4. Formation of 7 planar images. Volume of breast between detectors is divided into 7 equal slices. Point of interaction of LOR with 7 planes is used to localize event in that plane. Final image set consists of 7 frames, each of which corresponds to 1 slice.

slice closest to the upper PEM detector. The slice closest to the site of maximum focal uptake of FDG has the best-focused image of the tumor, allowing tumor localization in 3 dimensions. Figure 4 illustrates the formation of the planar images. This method of image formation is similar to that used in the early tomographic systems of the 1970s, except that the 7 images are obtained simultaneously and efficiency corrections are applied. The method has the advantage of producing the focal plane effect, as a result of which the image frame closest to the site of preferential glucose uptake has the most focused image of the 7. With prior knowledge of the thickness of the compressed breast, the distance of the tumor from the upper detector can be estimated. Data reconstruction is by limited-angle reconstruction and not by filtered backprojection. This method of data acquisition and image formation is extremely fast and enables partially live display of the emission images on the display monitor, facilitating subject repositioning if necessary. Emission images are displayed on an X-Windows color display on the host computer, which is an Alpha Station 200 (Compaq Canada, Kanata, Ontario, Canada). Windows for further analysis in the display program allow smoothing of images, drawing of profiles through different regions of interest, and scaling and overlaying of the emission image on the digitized mammogram (*29*).

Study Design

The goal of this clinical pilot study was to establish the diagnostic performance of the PEM-I system. To evaluate the technique, only 1 principal tumor mass was targeted. This mass was imaged with mammography and PEM, and the 2 images were coregistered. The actual state (malignant or benign) of the tumor was determined by pathologic assessment of the surgically removed tumor. The test state (PEM-positive or PEM-negative) was determined by the outcome of the PEM study. The sensitivity and specificity of both imaging modalities (mammography and PEM) were compared with the results of the final pathologic evaluation of the mass.

Subject Selection Criteria. The subjects were female, more than 18 y old, not diabetic, and not pregnant. They had both breasts intact and had recently been diagnosed with a suggestive mass in 1 breast. The mass had been detected by physical examination or mammography. The subjects had no medical history of cancer and no surgical intervention to preevaluate the histopathologic nature of the tumor before the PEM scan. Clinical scans followed guidelines set up by the Human Ethics Committee of the Royal Victoria Hospital. All subjects gave free and informed consent to the procedures and were allowed to withdraw from the studies at any time. In accord with the protocol, all subjects underwent surgical removal of the breast lesion within 2 wk after the PEM scan.

Subject Population. Candidates for PEM study were selected by 1 of the authors from subjects referred to the surgical oncology group at the Cedars' Breast Clinic of the Royal Victoria Hospital. Sixteen subjects were studied, and 14 studies were evaluable. One subject was excluded because a malfunction of the equipment led to abnormally low count-rates; the other subject was excluded because a core biopsy of the mass had been done 10 d before the PEM examination. All subjects but 1 presented with a palpable mass. All but 1 had mammographically visible tumors. All mammograms were read by the same radiologist and were classified on the basis of tumor shape, presence of microcalcifications, and other factors. These readings were independent of the PEM study and were not considered during subject accrual.

Clinical FDG Protocol. The subjects were instructed to fast for a minimum of 4 h before the injection of 75 MBq FDG in the arm contralateral to the breast with suggestive findings. Approximately 30 min after injection, the subjects were given water to drink and encouraged to void shortly before the PEM scan to eliminate the activity accumulated in the bladder—a major source of scatter radiation. PEM scanning was performed 45 min after injection. Patients received injections in the nuclear medicine department and were then taken to the breast clinic. No precautions were taken to minimize physical activity or cognitive tasks.

Scanning Sequence. Each subject was positioned on the mammography unit with the breast on the magnification table under minimal compression and the tumor mass at the center of the FOV. The PEM detectors remained outside the FOV, as illustrated in Figure 2A, and the coregistration tool was within the FOV. A mammogram of the breast was acquired. In the processed film, the white outline of the wire tool was clearly visible. If the tumor mass was not within the area outlined by the wire tool, the subject was repositioned. The mammogram was digitized.

The PEM detectors were slid into position as directed by the coregistration tool, as illustrated in Figure 2B, and emission data were acquired for up to 5 min. Emission data from the contralateral breast were acquired for comparison and to estimate the uptake in the presumed normal breast.

The mammogram was a magnified view because the breast was placed on the magnification table 25 cm above the film cassette. PEM images were not magnified. To overlay the 2, the best-focused PEM image was scaled to match the mammogram and the 2 images

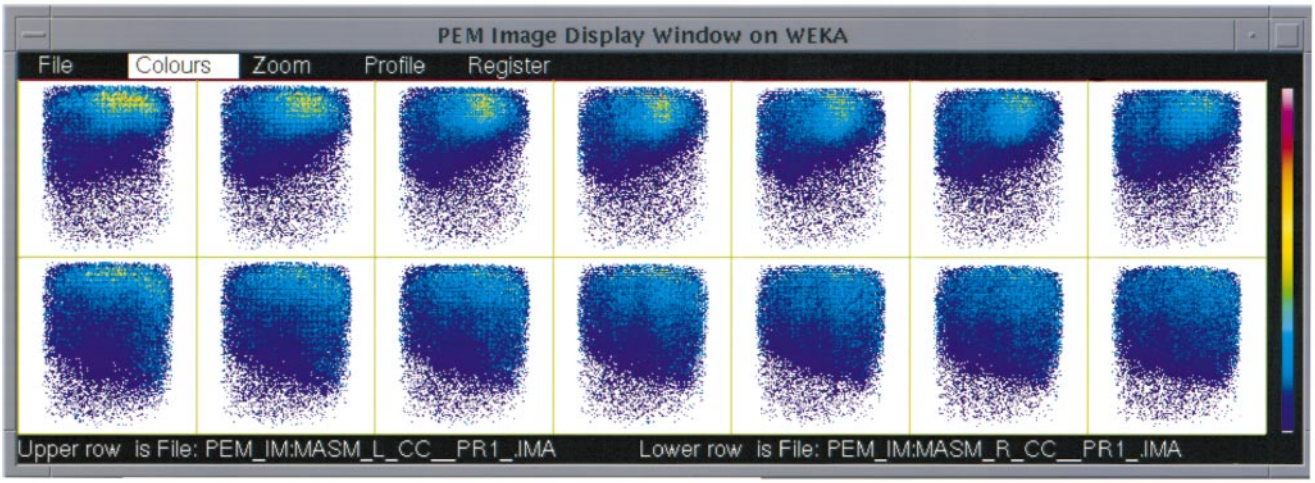

FIGURE 5. Typical set of true-positive PEM-I images, with upper row showing 7 emission images from breast with suggestive findings and lower row showing images from contralateral breast. Each image frame represents 1 slice through breast, with upper edge of frame corresponding to region of breast closest to chest wall and leftmost frame corresponding to image plane closest to upper detector. Localized region of preferential FDG uptake is visible in upper set of images. Pathologic evaluation of excised mass revealed infiltrating and intraductal carcinoma (2.5 × 2.2 × 2.2 cm, histologic grade 3 [Bloom Richardson], nuclear grade III).

were overlaid. The image coregistration technique has been described in detail (*28*).

Data Analysis

Emission images were displayed as 2 sets of 128 × 128 pixel images (corresponding to the 2 breasts), each consisting of 7 separate frames displayed in a 7 × 2 matrix. The first row of 7 images corresponded to slices through the breast with suggestive findings, and the lower row corresponded to slices through the contralateral breast. Figure 5 shows a typical image display during clinical scans. Image were reconstructed on-line, and images were updated at 5-s intervals. PEM data were classified as positive (indicating the presence of cancer) if significant focal uptake was seen in the region corresponding to the tumor mass compared with uptake in the background. Otherwise, the study was classified as negative (indicating the absence of cancer). This hot-spot imaging technique is widely used in PET when full image quantification is not performed. In our instance, visual diagnosis was further complemented semiquantitatively by drawing a profile through the hot spot and comparing it with a profile drawn through the background. On the basis of studies performed with a customized breast phantom (*27*), a count ratio of at least 2:1, hot spot to background, was taken to signal positive PEM findings.

Regardless of the outcome of visual inspection, emission data were further analyzed to determine whether significant count asymmetry existed between the 2 breasts. This analysis was a semiquantitative assessment of activity uptake. For both breasts, retroactive corrections had to be applied to account for physical decay of the source between the scans, the volume of breast tissue that was in the FOV at the time of scanning, and the detector separation used for each breast. The total number of counts detected from each breast was then normalized using these correction factors to get the average count for each breast. On the basis of receiver operating characteristic analysis (*31*), the breast with suggestive findings was classified as positive when the count asymmetry was greater than a 10% threshold.

Figure 6 shows the coregistered image of the suggestive breast of a true-positive PEM study. The best-focused emission (PEM) image (in color) from the set of 7 slices shown in the upper row in Figure 5 is scaled and superimposed on the digitized mammogram shown in gray scale. The white outline of the wire frame is used to scale the emission image to match the mammogram.

RESULTS

Early in this study, we recognized that the PEM instrument was incapable of imaging lesions within 2 cm of the chest wall. This factor limited and delayed our subject accrual rate. Of the 14 evaluable subjects (age range, 34–75 y; median age, 54.8 y), 10 were found to have cancerous tumors and 4 had benign lesions. Previous studies using a

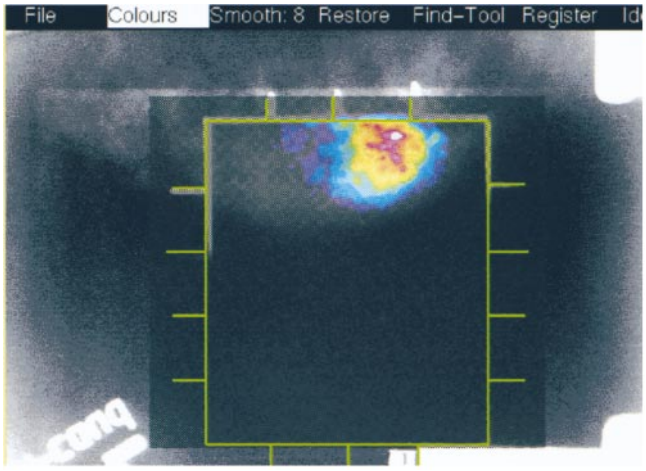

FIGURE 6. True-positive PEM image in pseudocolor overlaid on its corresponding mammogram in gray scale. Outline of coregistration tool, which appears white on mammogram (shown in green here), is used to scale best-focused PEM image. That image is then overlaid on mammogram. Top of image corresponds to region closest to chest wall of subject; left side of image corresponds to left side of imaged breast.

custom-built breast phantom showed the activity uptake in the heart to have a negligible effect on tumor contrast resolution (*32*).

Qualitative assessment of PEM images showed a clear region of focal uptake in 5 of 14 subjects, with a mean image contrast (ratio of hot spot to background) of 5.8:1. Count asymmetry between the 2 breasts was estimated for all 14 subjects. On the basis of receiver operating characteristic analysis, an asymmetry threshold of 10% was chosen as suitable for classification of the PEM findings as positive or negative. In 3 additional subjects, findings showing no apparent focal uptake were evaluated as PEM positive on the basis of count asymmetry. The average count asymmetry in these 3 subjects was 40% ± 15%. In all, 8 of 10 disease-positive subjects, (i.e., subjects diagnosed with cancer by surgical biopsy) were recognized with PEM. The average count asymmetry in these 8 subjects was 27%. Count asymmetry was clearly present in 3 of 5 subjects (average, 30%) and borderline in 1 other (9%) with a visible image abnormality. No significant asymmetry was evident in the 4 subjects with true-negative findings. No false-positive results occurred. Sensitivity, specificity, and accuracy were estimated using standard formulas. Table 1 compares the results from the 2 imaging modalities. Sensitivity based on imaging alone (no count-rate asymmetry) was 50%. Details about tumor histopathology and size are given in Table 2. The average tumor size was 2.0 × 1.6 × 1.6 cm, and the smallest detected tumor was 1.1 × 1.1 × 0.9 cm.

Neither of the 2 subjects with false-negative findings showed a prominent region of preferential uptake. One could not be assessed on the basis of count asymmetry because surgery (performed because of a recurrent cyst) on the contralateral breast revealed malignant tumors in both breasts. The other showed only an 8% count asymmetry.

DISCUSSION

The purpose of this pilot study was to test the clinical usefulness of the prototype system dedicated to breast imaging. Our limited data suggest that PEM can accurately detect cancerous lesions 80% of the time. When visual localization of uptake was used as the sole criterion for tumor diagnosis, the sensitivity of PEM was considerably lower (50%). The sensitivity of mammography was significantly higher, at 90%. On the other hand, the PEM-I system specificity was substantially greater than that of the mammography system (100% specificity compared with 81% for mammography). The capacity to produce coregistered emission and radiographic images of the breast tumor in the same sitting is an important but not essential feature of our system. In this limited trial, tumor diagnosis by PEM-I was consistently better than that by mammography. For 86% of subjects, PEM-I correctly established the presence or absence of cancer, whereas mammography could do so for only 78% of subjects.

TABLE 1
Comparison of PEM and Mammography Results

Index	Method of calculation	Imaging modality (%)	
		PEM	Mammography
Sensitivity	TP/(TP + FN)	80	90
Specificity	TN/(FP + TN)	100	50
Accuracy	TP + TN/(TP + TN + FP + FN)	86	78
Positive predictive value	TP/(TP + FP)	100	81
Negative predictive value	TN/(TN + FN)	67	67

TP = true-positive; FP = false-positive; FN = false-negative; TN = true-negative.

The principal drawbacks of the system are its limited access to regions close to the chest wall and its small FOV. Tumors closer than 2 cm from the chest wall are outside the FOV of the detectors and hence cannot be imaged successfully. This limitation is caused by the curvature of the glass envelope and the size of the anode wire matrix, which prevent identification of crystals near the edge of the PS-PMT, and by enclosure of the PS-PMT in a lighttight box that slides on rails into and out of the magnification table. The support structure for the lower detector box and the shielding around the crystals to exclude scatter radiation introduce a 1-cm-wide dead space between the detectors and the chest wall. Additionally, the sensitivity of the instrument falls as annihilations occur farther from the center of the FOV. Although the loss of efficiency is compensated for, the focal plane effect is not as great and the images are noisier at the edges than at the center. Planned improvements to the existing system, including modifications to the detector support system and offset imaging, will reduce the distance to 1 cm from the chest wall. The small-FOV problem is directly related to the type of PS-PMT used in this application (R3941-05). These PS-PMTs cannot image to their edge; hence, their useable area is considerably smaller than their physical area. Since the construction of this prototype, several newer models have become available that can image closer to their periphery.

For images that showed focal uptake, the average image contrast was 5.8:1. For a compressed breast thickness of 70 mm and a spherical 1.5-cm-diameter tumor, this ratio corresponds to a tumor-to-background uptake ratio of approximately 25:1 (*25*). Focal uptake in the form of a hot spot was seen in only 5 of 10 scans with true-positive findings, whereas count asymmetry was evident in 8 of 10, suggesting that semiquantitative analysis plays an important role in the diagnosis of cancer with PEM. Scanning parameters such as the thickness of the compressed breast, the interval between injection and imaging, and the image space occupied by the breast must be rigorously and consistently recorded for semiquantitative analysis to be accurate. Corrections for scanning parameters are now applied automatically.

We showed that small cancerous lesions could be detected with PEM-I quickly and with a relatively low dose of radioactivity. The smallest tumor detected was 1.1 × 1.1 ×

TABLE 2
Summary of Results

Subject no.	Mammography	PEM	Count rate difference* (%)	Pathology	Histology	
					Grade	Size (cm)
1	+	−	6	−	NA	3.2 × 2.6 × 2.2
2	−	+ (CA)	43	+	3	1.1 × 1.1 × 0.9
3	+	+ (HS + CA)	21	+	2	1.5 × 1.0 × 1.0
4	+	+ (HS + CA)	17	+	3	2.5 × 2.2 × 2.2
5	+	+ (CA)	22	+	2	5.5 × 4.5 × 2.8
6	+	+ (HS)	0	+	3	1.8 × 1.5 × 2.5
7	+	−	−4	−	NA	2.5 × 1.9 × 1.0
8	+	+ (HS + CA)	51	+	2	3.0 × 3.0 × 2.0
9	−	−	2	−	NA	1.5 × 1 × 1.2
10	+	+ (HS + CA)	9	+	3	1.5 × 1.5 × 1.3
11	+	−	−13	+	2	1.5 × 1.3 × 1.0
12	−	−	−21	−	NA	5.5 × 3.5 × 2.5
13	+	−	8	+	1	5.2 × 1.5 × 1.3
14	+	+ (CA)	53	+	2	1.2 × 1.0 × 1.2

*Difference between counts in breast with suggestive findings and counts in contralateral breast.
CA = count-rate asymmetry (>10% difference in count rates in breast with suggestive findings and contralateral breast); HS = tumor visible as hot spot in image.

0.9 cm. Most clinical breast imaging with PET has been performed on whole-body PET systems whose ring diameters must be large enough to accommodate the human torso (typically approximately 55 cm). Avril et al. (*17*) have studied 73 subjects and 97 breast tumors and have reported a sensitivity of 90% and a specificity of 85% for the ECAT-EXACT (CTI, Knoxville, TN) whole-body PET system using 370 MBq FDG and total scan times of 40–60 min for attenuation-corrected images. PEM images are acquired with a 5–10 times lower radiation dose of FDG compared with conventional PET, and imaging times are 8- to 12-fold shorter. The integration of only 2 detectors for PET into a mammographic instrument represents a cost savings from both the use of fewer detectors and the use of an existing imaging platform (the approximate cost of the instrument is $100,000). In addition to substantially higher efficiency because of the proximity of the detectors to the organ of interest, attenuation correction can be performed by simple scaling along the LORs because the compressed breast is of uniform thickness. Short imaging time and a low degree of breast compression aid in the subject's acceptance of this diagnostic technique. Further studies are required to confirm the diagnostic usefulness and clinical applicability of the PEM instrument.

CONCLUSION

We have shown that a dedicated system for the metabolic imaging of suggestive breast tumors can add useful information to that provided by conventional mammography and aid in the diagnosis of breast cancer. Accurate coregistration of emission images and mammograms is feasible and helpful in tumor localization. Our clinical experience has identified some limitations to the existing system that can be addressed with relative ease. Low radiation dose, short imaging times, and low cost make PEM a useful adjuvant to mammography. Apart from these, the advantages of such a system are its low cost because of the small number of detectors and its ability to display images on-line.

ACKNOWLEDGMENTS

The authors acknowledge the contributions of Dr. Michelle Auger, pathologist, Royal Victoria Hospital; Bonnie Courte, Jodie Ceccarelli, and Linda Matueszswska, Cedars' Breast Clinic, Royal Victoria Hospital; Dean Jolly, Medical Cyclotron Facility, Montreal Neurological Institute; and Lise Proulx, Department of Nuclear Medicine, Royal Victoria Hospital. This project was supported by grants 6139 and 9232 from the Canadian Breast Cancer Research Initiative of the National Cancer Institute of Canada.

REFERENCES

1. Harris KM, Vogel VG. Breast cancer screening. *Cancer Metastasis Rev.* 1997;16: 231–262.
2. Henson DE, Riess LA. Progress in early breast cancer detection. *Cancer*. 1990;65:2155–2158.
3. King SE, Schottenfeld D. The "epidemic" of breast cancer in the U.S.: determining the factors. *Oncology*.1996;10:453–462.
4. Kerlikowske K, Grady D, Barclay J, Sickles EA, Ernster V. Effect of age, breast density and family history on the sensitivity of first screening mammography. *J Am Med Assoc*. 1996;276:33–38.
5. National Institutes of Health Consensus Development Panel. *National Institutes of Health Consensus Development Conference Statement: Breast Cancer Screening for Women 40–49, Jan 21–23, 1997.* Vol 22. Washington, DC: National Cancer Institute; 1997:vii–xviii.
6. Schiepers C, Hoh CK. Positron emission tomography as a diagnostic tool in oncology. *Eur Radiol.* 1998;8:1481–1494.
7. Silverman DH, Hoh CK, Seltzer MA, et al. Evaluating tumor biology and oncological disease with positron-emission tomography. *Semin Radiat Oncol.* 1998;8:183–196.
8. Maublant J. Scintigraphic imaging of breast tumors. *Eur J Radiol*. 1997;24:2–10.

9. Mastin ST, Drane WE, Harman EM, Fenton JJ, Quesenberry L. FDG SPECT in patients with lung masses. *Chest.* 1999;115:1012–1017.
10. Taillefer R. The role of ^{99m}Tc-sestamibi and other conventional radiopharmaceuticals in breast cancer diagnosis. *Semin Nucl Med.* 1999;29:16–40.
11. Warburg O, Wind F, Neglers E. *On the Metabolism of Tumors in the Body*. London, UK: Constable; 1930:254–270.
12. Flanagan FL, Dehdashti F, Siegel BA. PET in breast cancer. *Semin Nucl Med*. 1998;28:290–302.
13. Adler DD, Wahl RL. New methods for imaging the breast: techniques, findings and potential. *AJR.* 1995;164:19–30.
14. Schneidhauer K, Scharl A, Pietrzyk U, et al. Qualitative [^{18}F]FDG positron emission tomography in primary breast cancer: clinical relevance and practicability. *Eur J Nucl Med.* 1996;23:618–623.
15. Wahl RL, Cody RL, Hutchins GD, Mudgett EE. Primary and metastatic breast carcinoma: initial evaluation with PET with radiolabeled ^{18}F-fluorodeoxyglucose PET. *Radiology.* 1991;197 765–770.
16. Crowe JP Jr, Adler LP, Shenk RR, Sunshine J. Positron emission tomography and breast masses: comparison with clinical, mammographic, and pathological findings. *Ann Surg Oncol*. 1994;1:132–140.
17. Avril N, Bense S, Ziegler S, et al. Breast imaging with fluorine-18-FDG PET: quantitative image analysis. *J Nucl Med.* 1997;38:1187–1190.
18. Avril N, Dose J, Janicke F, et al. Metabolic characterization of breast tumors with positron emission tomography using F-18 fluorodeoxyglucose. *J Clin Oncol*. 1996;14:1848–1857.
19. Freifelder R, Karp JS. Dedicated PET scanners for breast imaging. *Phys Med Biol.* 1997;42:2463–2480.
20. Levin CS, Hoffman EJ, Tornai MP, MacDonald LR. PSPMT and photodiode designs of a small scintillation camera for imaging malignant breast tumors. *IEEE Trans Nucl Sci*. 1997;44:1513–1520.
21. Singh M, Mumcuoglu E. Design of a CZT based breast SPECT system. *IEEE Trans Nucl Sci*. 1998;45:1158–1165.
22. Pani R, Scopinaro G, Pellegrini F, et al. Dedicated gamma camera for single photon emission mammography (SPEM). In: Nalcioglu O, ed. *IEEE Nuclear Science Symposium and Medical Imaging Conference.* Vol 2. Piscataway, NJ: IEEE;1997:1615–1619.
23. Weinberg I, Majewski S, Weisenberger A, et al. Preliminary results for positron emission mammography: real-time functional breast imaging in a conventional mammography gantry. *Eur J Nucl Med*. 1996;23:804–806.
24. Thompson CJ, Murthy K, Weinberg IN, Mako F. Feasibility study for positron emission mammography. *Med Phys.* 1994;21:529–538.
25. Murthy K, Aznar M, Bergman AM, et al. Positron emission mammographic instrument: initial results. *Radiology.* 2000;215:280–285.
26. Clancy RL, Thompson CJ, Robar JL, Bergman AM. A simple technique to increase the linearity and field-of-view in position sensitive photomultiplier tubes. *IEEE Trans Nucl Sci*. 1997;44:494–498.
27. Murthy K, Jolly D, Aznar M, et al. Quantification in positron emission mammography (PEM) with planar detectors: contrast resolution measurements using a custom breast phantom and novel spherical hot-spots. *IEEE Trans Nucl Sci*. 1999;46:2192–2196.
28. Robar JL, Thompson CJ, Murthy K, Clancy R, Bergman AM. Construction and calibration of detectors for high resolution metabolic breast cancer imaging. *Nucl Inst Meth Phys Res.* 1997;A392:402–406.
29. Bergman AM, Thompson CJ, Murthy K, et al. Technique to obtain positron emission mammography images in registration with x-ray mammograms. *Med Phys.* 1998;25:2119–2129.
30. Thompson CJ, Murthy K, Picard Y, et al. Positron emission mammography (PEM): a promising technique for detecting breast cancer. *IEEE Trans Nucl Sci*. 1995;42:1012–1017.
31. Metz C. Basic principles of ROC analysis. *Semin Nucl Med*. 1978;8:283–298.
32. Murthy K, Jolly D, Aznar M, et al. Quantification in positron emission mammography (PEM) with planar detectors: contrast resolution measurements using a custom breast phantom and novel spherical hot-spots. In: *Proceedings of the 1998 IEEE Medical Imaging Conference*. Piscataway, NJ: IEEE;1998:paper M7-46.

The Journal of NUCLEAR MEDICINE

Results of Preliminary Clinical Trials of the Positron Emission Mammography System PEM-I: A Dedicated Breast Imaging System Producing Glucose Metabolic Images Using FDG

Kavita Murthy, Marianne Aznar, Christopher J. Thompson, Antoine Loutfi, Robert Lisbona and Jean H. Gagnon

J Nucl Med. 2000;41:1851-1858.

The Journal of Nuclear Medicine is published monthly.
SNMMI | Society of Nuclear Medicine and Molecular Imaging
1850 Samuel Morse Drive, Reston, VA 20190.
(Print ISSN: 0161-5505, Online ISSN: 2159-662X)

SNMMI SOCIETY OF NUCLEAR MEDICINE AND MOLECULAR IMAGING